Contents lists available at ScienceDirect

Chemical Engineering Research and Design

journal homepage: www.elsevier.com/locate/cherd

Mixing by solid particles

J.J. Derksen

Chemical & Materials Engineering Department, University of Alberta, Edmonton, Alberta, T6G 2G6 Canada

ABSTRACT

A procedure for the direct numerical simulation (DNS) of the mixing of a passive scalar dissolved in a fluid phase due to the motion of spherical solid particles relative to the fluid is outlined. The procedure is based on solving the fluid flow in between the solid spheres with the lattice Boltzmann method, a molecular dynamics type of approach for the solid particle motion (including hard-sphere collisions), and solving a convection–diffusion equation for the passive scalar. The full resolution (in terms of particle motion, flow of interstitial fluid, boundary conditions at the particle surfaces) implies that only small-scale systems can be considered. In this paper the procedure is applied to a fully periodic system to assess the mixing performance of granular particles, and to a micro-channel in which particles are contained to enhance scalar mixing in laminar flow.

Keywords: Scalar mixing; Multiphase flow; Direct numerical simulation; Granular dynamics

1. Introduction

In many chemical and environmental engineering applications, dense gas–solid and liquid–solid flows are encountered frequently. If species are dissolved in the fluid phase, they get dispersed and mixed by fluid flow and molecular transport with the flow driven by multiple sources, the motion of the particles relative to the fluid being one of them. In order to model the transport of a scalar in the fluid phase, somehow the role of the particles in the dispersion of the scalar needs to be taken into account. So far this modeling is largely based on empirical dispersion models as they can be found in e.g. the monograph by Levenspiel (1962) and references therein. Also – in the context of computational fluid dynamics (CFD) of turbulent disperse multiphase flows – it is quite common to apply the analogy of transport of momentum by eddies and of a scalar for estimating scalar eddy diffusion/dispersion coefficients. It is questionable if such an approach would be valid for systems with high volumetric disperse phase loadings (where turbulence can hardly develop due to the small interparticle spacings), and applications involving laminar flow such as (multiphase) micro-reactors.

In the present study, numerical experiments are described that directly probe the spreading of a passive scalar as a result of solid particle motion. The moving particles agitate the interstitial fluid. Subsequently the flow disperses the scalar dissolved in the fluid. Goals of the simulations are to find out how the scalar spreading scales with the parameters governing the particle and fluid motion such as the granular temperature. Due to the level of detail that needs to be resolved in the simulations, we have to limit ourselves to small systems (in terms of the volume and/or the number of particles involved). Two sets of cases will be considered in this paper. In one set of cases we take a small, fully periodic, three-dimensional system that we 'stir' by solid, spherical particles that move through the fluid as a granular gas (i.e. they agitate the interstitial fluid without their motion being affected by the presence of the fluid). This mimics a homogeneous system in which we single out the effect of particle motion on scalar dispersion. The other set of cases relate to micro-channels that e.g. could be part of a micro-reactor. In such channels mixing is an inherent problem given the low Reynolds numbers inhibiting turbulent structures to develop.

In the systems we study numerically, the motion of the solid particles and the interstitial liquid are fully resolved, including finite-particle-size effects. In the cases involving micro-channels, particle motion and fluid flow are fully coupled, i.e. the moving particles initiate fluid flow; the hydrodynamic forces stemming from fluid flow act on the particles and influence their motion. In the granular cases (with fully periodic boundary conditions) the particles move as a granular gas with a constant temperature. As mentioned above, the particles do not feel the presence of the fluid. At the fluid–solid interfaces, however, we impose a no-slip condition

E-mail address: jos@ualberta.ca.

Received 7 July 2008; Accepted 14 July 2008

0263-8762/$ – see front matter © 2008 The Institution of Chemical Engineers. Published by Elsevier B.V. All rights reserved.

doi:10.1016/j.cherd.2008.07.007

Nomenclature

c, c_0	scalar concentration, initial scalar concentration
$c_{z<H/2}$	average scalar exit concentration in half the channel
$\tilde{c}(x, t)$	one-dimensional scalar concentration function
d_p	particle diameter
f_c	collision frequency
$\mathbf{g}$	gravitational acceleration vector
H	channel width
L	linear size of 3D periodic domain
L_b, L_d, L_u	channel portions (bed, downstream, and upstream length, respectively)
M	number of realizations
N	number of particles
$\mathbf{r}_p$	particle center position
$Re_{ch} = u_{in}H/\nu$	channel Reynolds number
$Re_g = \sqrt{T_g}d_p/\nu$	granular Reynolds number
$Sc = \nu/\Gamma$	Schmidt number
T_g	granular temperature
t	time
u_{in}	inlet velocity
$\mathbf{v}_p$	particle velocity
v_s	particle settling velocity
x, y, z	spatial coordinate system
α	fitting parameter
Γ, Γ_e	diffusivity, effective diffusivity
ϕ	solids volume fraction
λ	mean-free-path
ν	kinematic viscosity
ρ_s, ρ_l	solid and liquid density
σ	scalar concentration profile width
$\mathbf{\Omega}_p$	particle angular velocity

on the fluid. In that manner the fluid responds to the particle motion and gets agitated. In all simulations discussed, collisions of particles are explicitly resolved and considered to be fully elastic and smooth (no friction). Once the fluid–solid systems are fully developed, we release a passive scalar in the fluid phase. By solving the convection–diffusion equation for the tracer with non-penetration boundary conditions at the solid surfaces, we observe how the tracer spreads by the action of the moving solid particles. We do not consider mass transfer between the particles and the fluid, the solid particles are there to agitate the fluid and thus mix the scalar dissolved in the fluid phase. To limit the parameter space, we give the dissolved scalar a high Schmidt number, i.e. we set the molecular diffusivity of the passive scalar close to zero. The (inevitable) numerical diffusion is suppressed by using a total variation diminishing (TVD) scheme in estimating convective fluxes (Harten, 1983). The level of numerical diffusion has been assessed by checking the effect of grid refinement.

2. Numerical procedure

The lattice-Boltzmann method (LBM) (Chen and Doolen, 1998; Succi, 2001; Yu et al., 2003) has been used to solve the fluid flow in between the spherical particles. In the micro-channel cases, fluid and particle motion are fully coupled by demanding that at the surface of each sphere the fluid velocity matches the local velocity of its surface (which is the sum of the linear velocity $\mathbf{v}_p$, and rotation $\mathbf{\Omega}_p \times (\mathbf{r} - \mathbf{r}_p)$ with $\mathbf{\Omega}_p$ the angular velocity of the sphere, $\mathbf{r}_p$ the center position of the sphere, and $\mathbf{r}$ a point on its surface). In the forcing scheme that is applied here for establishing no-slip at the spherical surfaces this is accomplished by imposing additional forces on the fluid at the surface of the solid sphere. The details of the implementation can be found elsewhere (Goldstein et al., 1993; Derksen and Van den Akker, 1999; Ten Cate et al., 2002). The collection of forces representing the no-slip conditions is added up to determine the hydrodynamic force and torque acting on each sphere (action = −reaction). For the non-granular cases these are used to evaluate the equations of linear and rotational motion of the spheres. Sphere–sphere (and sphere–wall collisions in case of micro-channel flow) are considered fully elastic and smooth (no friction). In the granular cases, smooth and elastic collisions imply a constant granular temperature.

The dispersion of the passive scalar dissolved in the continuous phase fluid is simulated by numerically solving a convection–diffusion equation for the scalar concentration c. For this an explicit finite volume representation on the same grid as used by the LBM is employed. To limit numerical diffusion, we apply TVD discretization with the Superbee flux limiter for the convective fluxes (Sweby, 1983). We step in time according to an Adams–Bashford scheme. We do not allow scalar concentration inside the spherical particles. At the surface of the particles we impose $\partial c/\partial n = 0$. This condition is also applied for assigning concentrations to grid nodes that get uncovered by a moving solid particle. Since particles typically move less than 0.05 times the lattice spacing per time step, an uncovered node always is close to a solid particle interface. We draw the normal out of the particle into the fluid at the position of the uncovered node. By interpolation we determine the concentration on the normal one additional grid spacing into the fluid and assign that concentration to the uncovered node (see Hartmann et al. (2006) for more details). In some situations this procedure cannot be followed: it regularly occurs that a grid cell gets uncovered in between two closely spaced particles moving away from each other after a collision. In such cases we assign the average concentration in the direct vicinity to the uncovered grid node, while keeping that vicinity as small as possible. Particles covering and uncovering grid nodes containing scalar mass makes the simulations not inherently mass conservative. In practice, total scalar mass is conserved within a 0.5% uncertainty range.

3. Micro-channel simulations

We consider vertically placed channels with square cross sections (see Fig. 1). At the bottom of the channel we force fluid in by imposing a uniform velocity u_{in} over the cross sectional area. This velocity, the channel size H and the fluid viscosity ν define the channel's Reynolds number: $Re_{ch} = u_{in}H/\nu$. In the channel we place uniformly sized spherical particles with diameter d_p. The particles are confined to a section of the channel with length L_b. They move freely around this space. At its lower and upper end the particles collide on an imaginary wall that the fluid passes undisturbed. These boundaries can be viewed as very fine wire meshes (with mesh width much smaller than d_p). Upstream and downstream of the bed the channel is void of particles over length L_u and L_d, respectively (see Fig. 1)

The dimensionless numbers governing the particle system are the solids volume fraction ϕ of the particle bed, the aspects ratios d_p/H and L_b/H, and the solid over fluid density ratio ρ_s/ρ_l.

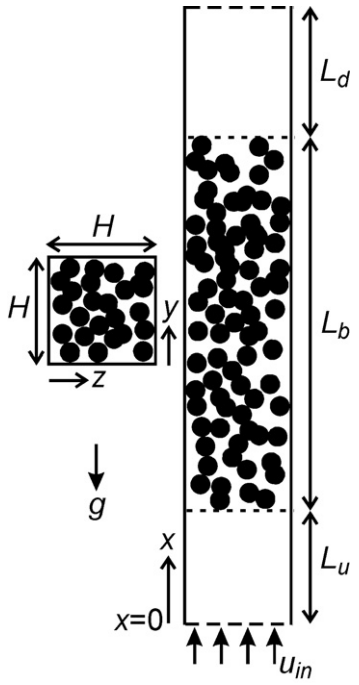

Fig. 1 – Micro-channel flow geometry including definition of the coordinate system. The vector g indicates the direction of gravity and is in the negative *x*-direction.

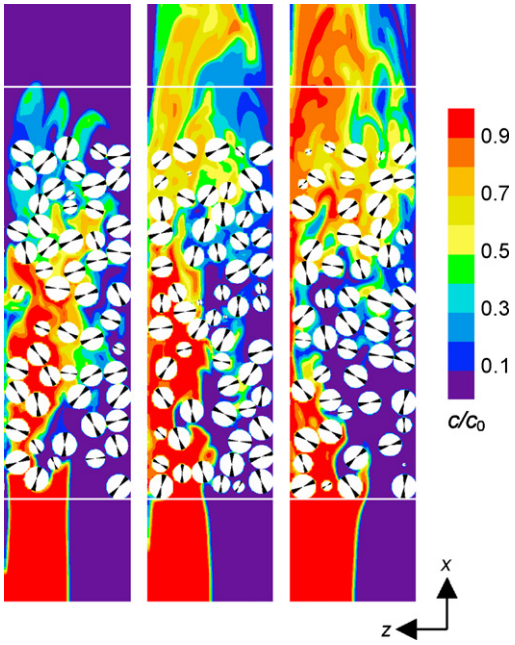

Fig. 2 – Scalar concentration in the center *xz*-plane of the micro-fluidized bed at three moments in time ($t = 2, 4, 8 \times H/u_{in}$) after starting the release of the scalar at $x = 0$. Conditions: $\phi = 0.365$, $v_s/u_{in} = 24$, $Re_{ch} = 12.2$.

Finally, since we will be considering cases with fluidized particles in vertical channels gravitational acceleration **g** plays a role. It is introduced via the Stokes settling velocity of a single particle in unbounded fluid $v_s = 1/18(\rho_s - \rho_l)\left|\boldsymbol{g}\right|/(\rho_l \nu) d_p^2$ included in the velocity ratio v_s/u_{in}.

Scalar mixing is quantified by solving the convection–diffusion equation for a passive scalar concentration c with scalar diffusivity Γ (and Schmidt number $Sc = \nu/\Gamma$) dissolved in the liquid. The scalar enters fully segregated at the bottom side (at $x = 0$) of the mixer: in half of the inlet cross section ($z < H/2$), no scalar is added; in the other half of the inlet cross-section ($z > H/2$) we maintain a scalar concentration of $c = c_0$. The scalar release at $x = 0$ only starts when the solid–liquid flow is fully developed; the start of scalar release is denoted with $t = 0$. Two dimensionless groups were a priori set constant: $\rho_s/\rho_l = 2.5$ (e.g. solid glass beads in water), the Schmidt number was set to 10^3 (hardly any molecular diffusion).

3.1. *Results*

Typical laminar flow results ($Re_{ch} = 12.2$) in terms of evolving concentration fields for a fluidized bed case are given in Fig. 2. We look at the center cross section through the channel at three moments after the scalar release. The round disks are the cross sections of the spheres; all spheres have the same size but are positioned differently with respect to the cross section. We keep track of the orientation of the spheres (indicated by the black markers on each sphere). The thin, horizontal white lines in the panels are the boundaries the spheres are confined to. In Fig. 3 is a snapshot of the scalar concentration fields in the exit plane after steady state almost has been reached. It clearly shows that at the exit the scalar field has not completely forgotten its segregated state in which it entered.

The motion of the fluidized particles induces fluid motion that helps in dispersing the scalar. Particle motion induces temporal variation in the scalar field as shown in the time series of the average concentration in the exit plane (Fig. 4).

A simple way to characterize scalar dispersion is by monitoring at the exit plane how much scalar has reached the side of the channel with $z < H/2$, i.e. that part of the channel's cross-section where no scalar was injected at the inlet plane. We quantify this with the average scalar concentration over that part of the exit plane with $z < H/2$ (denoted as $c_{z<H/2}$). A value of $c_{z<H/2} = 0$ implies no dispersion at all; a value of $0.5c_0$ implies ideal dispersion since in that case the exit concentration must be virtually uniform. Time series of $c_{z<H/2}$ have been included in Fig. 4. They show a time-averaged value of $0.291c_0$ (and standard deviation $0.043c_0$) for the fluidized case in quasi steady state (reached after $tu_{in}/H \approx 10$).

Increasing the length of the channel helps in better spreading the scalar. In Fig. 5a we show $c_{z<H/2}$ for three lengths of the reactor, with the same further conditions. The exit concentration increases; its standard deviation decreases with length. The exit concentration $c_{z<H/2}$ can be translated in an effective diffusion (or dispersion) coefficient by means of a simple,

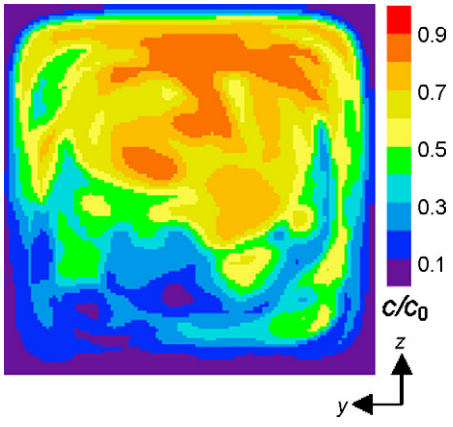

Fig. 3 – Scalar concentration in the exit plane at $t = 8\,H/u_{in}$. Same conditions as Fig. 2.

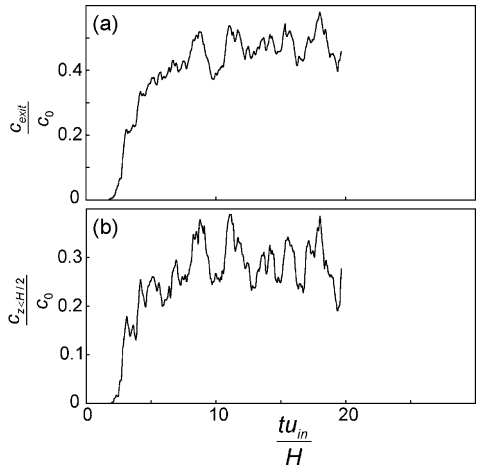

Fig. 4 – Time series of the average concentration in the exit plane (a), and lower portion of the exit plane (b) for the fluidized bed case as depicted and defined in Fig. 2.

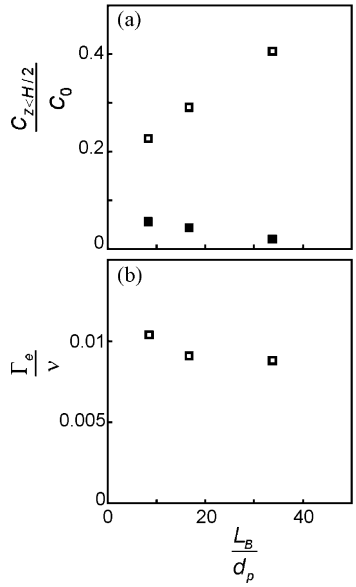

Fig. 5 – Time-average exit concentrations $c_{z<H/2}$ at quasi steady-state (a), and effective diffusivities (b) as a function of reactor length. The filled squares in (a) indicate the RMS of the fluctuations in quasi steady state.

one-dimensional diffusion model:

$$\Gamma_e = \frac{1}{4\pi}\left(\frac{c_{z<H/2}}{c_0}\right)^2 \frac{H^2 u_{in}\phi}{L_b} \quad (1)$$

The results in Fig. 5b show that Γ_e only weakly depends on L_b, giving some credit to the simple diffusion model.

4. Granularly moving particles

In order to generalize and extend the results with the micro-channels to bigger systems we now consider fully periodic, three-dimensional, cubic domains with edge length L. These mimic large homogeneous systems. In such cubic domains we release N spherical particles all having the same diameter d_p. The solids volume fraction of the system is $\phi = N\pi d_p^3/(6L^3)$. The particles are given a mean-square velocity of $2T_g$, with T_g the granular temperature. The energy of the particulate system is fully contained in translational motion – the particles do not rotate. The granular temperature is kept constant by letting the particles undergo fully elastic and frictionless hard-sphere collisions. After this (dry) granular system has evolved to a steady state, we introduce the interstitial fluid. This fluid is one-way coupled to the particles: the fluid responds to the particle motion; the particles do not feel the fluid and continue their granular motion. The flow dynamics of this system are characterized by two dimensionless numbers: the solids volume fraction ϕ, and the Reynolds number based on the granular temperature $Re_g = \sqrt{T_g} d_p/\nu$.

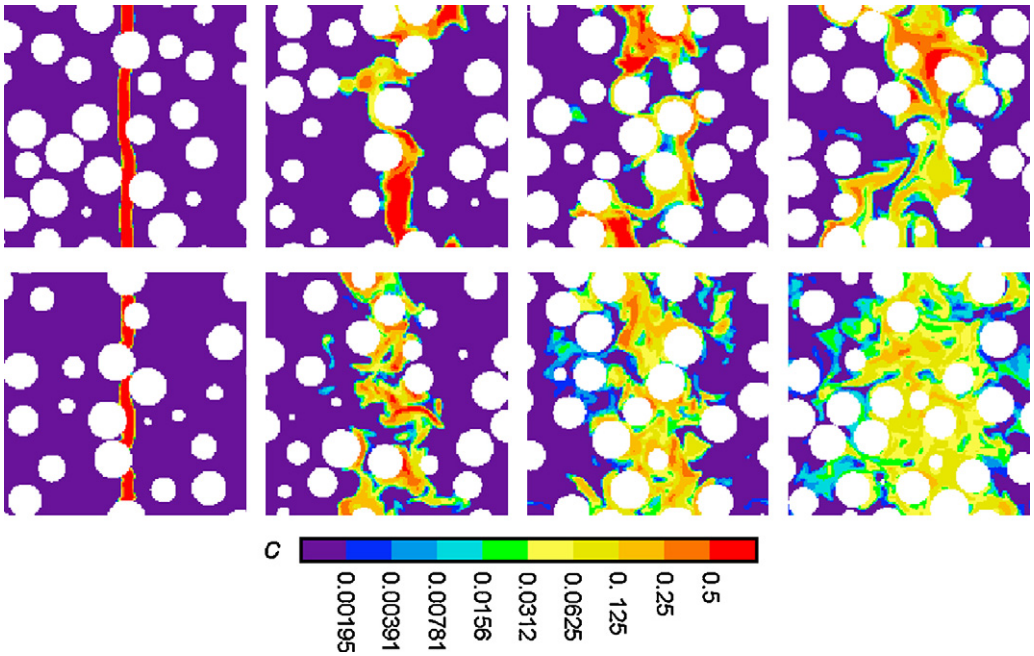

Fig. 6 – Snapshots of concentration contours in xz cross-sections through the cubic domain. Top four panels: $\phi = 0.30$ and $Re_g = 2.8$ at (from left to right) $t\sqrt{T_g}/d_p = 0.05$, 1.96, 3.88, and 5.79, respectively. Bottom four panels have the same parameters except now $Re_g = 104$.

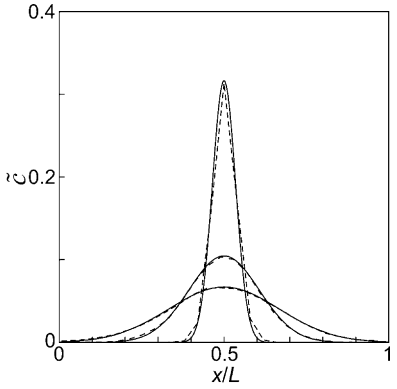

Fig. 7 – Simulated (dashed lines) and fitted (solid lines) one-dimensional concentration profiles at three instants in time: $t\sqrt{T_g}/d_p = 0.43$, 2.16, and 4.33. $\phi = 0.30$ and $Re_g = 104$.

We start simulating passive scalar transport once the flow is fully developed. As initial condition for the scalar concentration we give a thin yz-slab (with slab thickness $d_p/4$) of fluid a concentration $c = 1$, and the rest of the fluid $c = 0$. Subsequently we keep track of the spreading of the scalar as a result of the fluid flow induced by the solid particle motion. Typical sequences are given in Fig. 6.

The full, three-dimensional data are reduced to a one-dimensional scalar concentration function $\tilde{c}(x, t) \equiv 1/(L^2)\int_0^L\int_0^L c(x, y, z, t)dydz$. By repeating the simulation M times and averaging the results we get smooth $\tilde{c}(x, t)$ profiles that we fit with a Gaussian $\tilde{c}_{fit}(x, t) = a/(\sigma(t)\sqrt{2\pi})\exp((x-\mu)^2/2\sigma(t)^2)$, see Fig. 7. The default value of the number of repetitions M has been set to 20. The only fitting parameter is σ; the other two parameters (α and μ) are a priori known and constant in time. They relate to the total scalar mass being released (α), and the average position of the scalar μ (which is the center position of the initial slab). We use the way σ develops in time as a measure for the scalar dispersion.

In Fig. 7 we see that – compared to the later stages – for "short" times the simulated concentration profile does not fit a Gaussian very well. This is due to the top-hat initial concentration profile we imposed. At later stages, however, the profiles are very much akin to Gaussian functions, and the width of the fitted Gaussian is a good measure for the scalar spreading.

The solids volume fractions that have been considered are $\phi = 0.10$, 0.20, 0.30, 0.373, and 0.45. The cases with $\phi = 0.30$ served as base cases. Verification tests regarding reproducibility, grid refinement, time step, and domain size were performed at this volume fraction. For each volume fraction we vary the Reynolds number based on the granular temperature (Re_g) by varying the fluid viscosity. The Reynolds numbers considered are 2.8, 28, 104, and 280.

The default values for the particle diameter d_p is 16 lattice spacings ($d_p = 16$ in LB units). The default domain size $L = 100$ ($L = 6.25d_p$). The number of spheres in the computational domain determines ϕ. The granular temperature is chosen such that the solid particle velocities (a good measure of which is $\sqrt{T_g}$) stay well below the speed of sound of the lattice-Boltzmann scheme: T_g is of the order of 10^{-4}, the speed of sound is of order 1.

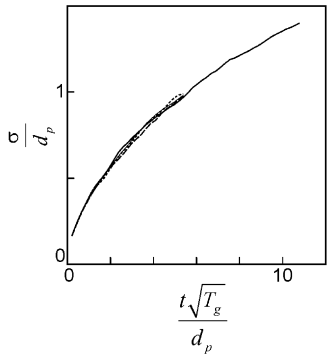

Fig. 8 – Concentration profile width σ as a function of time for three statistically independent repetitions with $\phi = 0.30$ and $Re_g = 2.8$ on a cubic L^3 domain (thin solid curve, dotted curve, dashed curve). The thick solid curve has the same settings except for the domain size in x-direction and the time span of the simulations. Both were doubled.

4.1. Results

A number of verification tests were performed for cases with $\phi = 0.30$. One of the things we checked was reproducibility, i.e. if the size of the ensemble M (=20) that we base our fitting procedure on is large enough to get reproducible results. In conjunction with reproducibility we checked the influence of the domain length in x-direction. As can be seen in Figs. 6 and 7, at some stage in time the concentration profile gets a width comparable to the size L of the domain. The periodic conditions then make the scalar leaving the domain on the right hand side enter on the left hand side, inhibiting a fit with a single Gaussian. One of the options for extending the time span of some of the simulations is enlarging the domain size in x-direction. Fig. 8 shows results on reproducibility and on the effect of doubling the domain size in x-direction in the form of evolutions of σ as a function of time. The σ versus t curves are well reproducible (deviations less than 4%). Extending the domain size allows for longer runs thus getting a clearer view on the functional relationship between the concentration profile width σ and time.

There is a very distinct effect of the solids volume fraction on scalar spreading. In Fig. 9 we show that the scalar spreading increases significantly with decreasing solids volume fraction. This is not a surprising result. The mean-free-path (MFP, symbol λ) defined – in analogy to kinetic theory and atomic physics – as the average distance solid particles travel in between two subsequent collisions, increases with decreasing solids

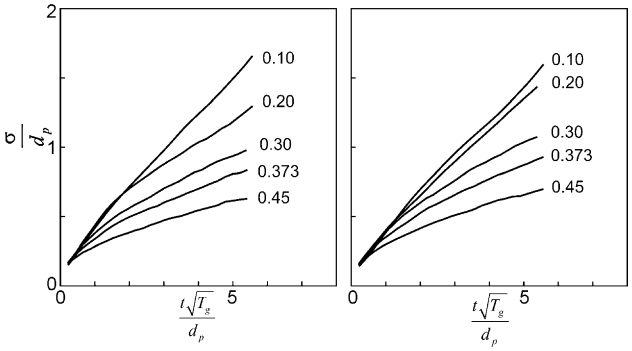

Fig. 9 – Concentration profile width σ as a function of time for various solids volume fractions. Left panel: $Re_g = 2.8$; right panel: $Re_g = 28$.

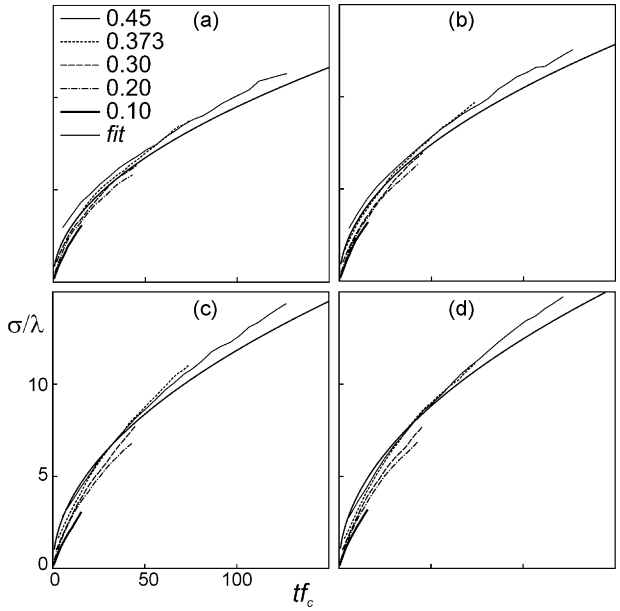

Fig. 10 – Concentration profile width σ as a function of time for various solids volume fractions. Time has been scaled with the collision frequency f_c, σ with the MFP λ. Panels a, b, c, and d, respectively, have $Re_g = 2.8$, 28, 104, and 280. The fit also included is the function $\sigma/\lambda = \sqrt{\alpha t f_c}$. The fitting parameter α differs per panel and is 0.9, 1.1, 1.4, and 1.5, respectively.

volume fraction (for dilute gases this is an inversely proportional relationship). If the particles are able to travel longer in a certain direction, they take with them the scalar over longer distances. This notion suggests that it makes sense to scale the scalar spreading as a function of time in terms of collisional parameters, viz. the MFP and the collision frequency of the particles. This we do in Fig. 10. It shows the scalar spreading as a function of time for all the four Reynolds numbers we have considered. The MFP λ and the collision frequency f_c were directly determined from the simulations. For each Reynolds number, the curves taken at different solids volume fraction get quite close to one another. There is a systematic difference though. The curves related to the higher solids volume fractions are slightly but systematically above the ones with lower ϕ; apparently the scaling with λ and f_c slightly overcompensates the differences as observed when scaling with d_p and $d_p/\sqrt{T_g}$ (as in Fig. 9).

Also shown in Fig. 10 is the (by the eye) best fit through the bundle of curves according to the function $\sigma/\lambda = \sqrt{\alpha t f_c}$, with α the only fitting parameter. We estimate this rather coarse way of fitting to be roughly $\pm 8\%$ accurate in α. We see that despite the uncertainties involved, the dimensionless parameter α clearly depends on the granular Reynolds number. For low Reynolds numbers the fluid flow and thus the scalar spreading are largely slaved to the kinematics of the particle motion; the flow does not develop structures smaller than those related to the particle field. At higher Reynolds numbers, the more inertial flow develops eddies that play a role in enhancing scalar spreading.

5. Summary

In this article we discussed mixing as a result of solid particle motion. We set up fully resolved simulations of a micro-channel with mixing enhanced by fluidized particles, and of fully periodic domains with granular particles. The latter mimics a homogeneous system with constant granular temperature. The amount of scalar spreading strongly depends on the solids volume fraction, with higher solids volume fractions leading to lower spreading; scalar spreading in terms of the width of the scalar concentration profiles is roughly proportional to the mean-free path of the solid particles.

The fluidized particles dispersed in micro-channels enhance laminar mixing, and may be an option to overcome the in many cases problematic scalar mixing in micro reactors. The simulations clearly need further work in the sense that a large parameter space (solids volume fraction, particle size relative to channel size, channel length, fluidization velocity) needs to be explored in order to design and optimize such micro mixing devices.

References

Chen, S. and Doolen, G.D., 1998, Lattice Boltzmann method for fluid flows. Annu Rev Fluid Mech, 30: 329–364.

Derksen, J.J. and Van den Akker, H.E.A., 1999, Large eddy simulations on the flow driven by a Rushton turbine. AIChE J, 45: 209–221.

Goldstein, D., Handler, R. and Sirovich, L., 1993, Modeling a no-slip flow boundary with an external force field. J Comput Phys, 105: 354–366.

Harten, A., 1983, High resolution schemes for hyperbolic conservation laws. J Comput Phys, 49: 357–393.

Hartmann, H., Derksen, J.J. and Van den Akker, H.E.A., 2006, Mixing times in a turbulent stirred tank by means of LES. AIChE J, 52: 3696–3706.

Levenspiel, O., (1962). *Chemical Reaction Engineering* (2nd edition). (Wiley, New York).

Succi, S., (2001). *The lattice Boltzmann Equation for Fluid Dynamics and Beyond*. (Clarendon Press, Oxford).

Sweby, P.K., 1983, High resolution schemes using flux limiters for hyperbolic conservation laws. SIAM J Num Anal, 21: 357–393.

Ten Cate, A., Nieuwstad, C.H., Derksen, J.J. and Van den Akker, H.E.A., 2002, Particle imaging velocimetry experiments and lattice-Boltzmann simulations on a single sphere settling under gravity. Phys Fluids, 14: 4012–4025.

Yu, D.Z., Mei, R.W., Luo, L.S. and Shyy, W., 2003, Viscous flow computations with the method of lattice Boltzmann equation. Prog Aerospace Sci, 39: 329–367.